Supplementary Information (SI) for Chemical Communications.
This journal is © The Royal Society of Chemistry 2026

Supporting Information

In Situ Electrocatalytic H_2O_2 Synthesis over TiO_2 Nanocrystal/Porous Carbon Yolk-Shell Composites with Oxygen Functional Group Modulation

Yue Tian[a], Jie Wang[a,b*], Tianhong Zhou[a], Shengchun Ma[b],Yusuke Yamauchi[b,c,*]

a. Key Laboratory of Integrated Regulation and Resource Development on Shallow Lakes, Ministry of Education, College of Environment, Hohai University, Nanjing 210098, China

b. Australian Institute for Bioengineering and Nanotechnology (AIBN), The University of Queensland, Brisbane, Queensland 4072, Australia

c. Department of Materials Process Engineering, Nagoya University, Furo-chou, Chikusa-ku, Nagoya 464-8601, Japan

**Corresponding author.*

E-mail: wang.jie@hhu.edu.cn (J. W.); y.yamauchi@uq.edu.au (Y. Y.)

Experimental sections

Synthesis of the samples

Synthesis of yolk-shell TNC/C-X sample: Glycerol ($C_3H_8O_3$, 10 mL), $TiOSO_4$ (1 mL), and diethyl ether ($C_2H_5OC_2H_5$, 8 mL) were added sequentially to ethanol (C_2H_5OH, 20 mL) under stirring and stirred for 15 min. The resulting mixture was transferred to a Teflon-lined stainless-steel autoclave and heated at 110 °C for 48 h. After cooling to room temperature, the white precipitate was collected by suction filtration, washed with ethanol three times, and dried at 60 °C overnight. The dried product was then calcined at 1000 °C for 2 h under an Ar atmosphere to obtain TP/C. For acid etching, TP/C (100 mg) was dispersed in H_2SO_4 (40 mL) and stirred for 10 min in a 50 mL Teflon liner. The mixture was sealed in a hydrothermal autoclave and heated at 160 °C for 4 h. After cooling, the resulting powder was collected by centrifugation, washed with deionized water three times, and dried at 60 °C for 12 h to yield TNC/C-4. By varying the hydrothermal reaction time (1, 3, or 10 h), the corresponding samples were denoted as TNC/C-1, TNC/C-3, and TNC/C-10, respectively.

Synthesis of the TNC/C-4-H_2: TNC/C-4 was further annealed at 600 ℃ for 2 h under 10% H_2/Ar atmosphere to obtain the reduced sample, denoted as TNC/C-4-H_2.

Characterizations

X-ray diffraction (XRD) patterns were collected on a Rigaku D/Max-2000 diffractometer using Cu Kα radiation (λ = 1.54 Å). Field-emission scanning electron microscopy (FESEM, HITACH S-4800 SEM) and transmission electron microscopy (TEM, JEM-2100) were used to examine the morphology and microstructure. X-ray photoelectron spectroscopy (XPS) measurement was performed on a Perkin Elmer PH 1500C instrument. Nitrogen adsorption-desorption isotherms were recorded on a Micromeritics TriStar II system at 77 K after degassing the samples at 120 °C for 6 h. The specific surface area was calculated using the Brunauer-Emmett-Teller (BET) method, and the pore size distribution was derived from the adsorption branch using

the Barrett-Joyner-Halenda (BJH) model. Thermogravimetric analysis (TGA) was carried out in air at a heating rate of 10 °C min^{-1}. Raman spectra were collected on a Dilor LabRam II system using a 633 nm He-Ne laser.

Electrochemical measurements: To prepare the working electrode, 5 mg of electrocatalyst was dispersed in 975 μL of ethanol and 25 μL of Nafion solution (5 wt.%) and sonicated for 1 h to form a homogeneous ink. Then, 10 μL of the ink was drop-cast onto a glassy carbon electrode (geometric area: 0.2475 cm^2) and dried under ambient conditions. Electrochemical measurements were performed on a CHI760E electrochemical workstation using a three-electrode configuration, with the catalyst-coated glassy carbon electrode as the working electrode, a graphite rod as the counter electrode, and an Ag/AgCl electrode as the reference electrode. Measurements were conducted in 0.1 M KOH or 0.1 M Na_2SO_4 aqueous solution. Prior to testing, the electrolyte was purged with high-purity O_2 or N_2 for at least 20 min. Cyclic voltammetry (CV) was performed at a scan rate of 50 mV s^{-1}. Linear sweep voltammetry (LSV) was recorded at 1600 rpm with a scan rate of 5 mV s^{-1}. All potentials were converted to the reversible hydrogen electrode (RHE) scale according to the following equation:

$$E_{RHE} = E_{Ag/AgCl} + 0.197 + 0.059 * pH$$

The H_2O_2 selectivity and electron-transfer number (n) were determined using a rotating ring disk electrode (RRDE) based on the disk current (I_D) and ring current (I_R). The collection efficiency (N) of the Pt ring was 0.38. The H_2O_2 selectivity (Sel.) and electron-transfer number (n) were calculated using the following equations:

$$Sel.(\%) = 200 * \frac{I_R / N}{I_D + I_R / N}$$

$$n = \frac{4 * I_D}{I_D + I_R/N}$$

H_2O_2 Quantification: The H_2O_2 concentration was determined by cerium sulfate titration ($Ce(SO_4)_2$). This method is based on the reduction of yellow Ce^{4+} to colorless Ce^{3+} by H_2O_2 according to the following reaction:

$$2\,Ce^{4+} + H_2O_2 \rightarrow 2\,Ce^{3+} + 2\,H^+ + O_2$$

Phenol Degradation Test: Electro-Fenton degradation of phenol was carried out in a three-electrode system using a CHI 760E workstation. The catalyst-coated glassy carbon electrode served as the working electrode, with a graphite rod as the counter electrode and an Ag/AgCl as the reference electrode. The electrolyte consisted of 0.1 M Na_2SO_4 containing 0.2 mM $FeSO_4$ and phenol at different initial concentrations. The applied potential was set to 0.2 V vs. RHE. A total of 50 mL of electrolyte was added into a 100 mL reaction cell, and the solution was purged with O_2 for 15 min prior to electrolysis. Aliquots were collected immediately after O_2 saturation and again after 10 min of electrolysis. Phenol concentrations were quantified by high-performance liquid chromatography (HPLC), and degradation efficiencies were calculated using a standard calibration curve.

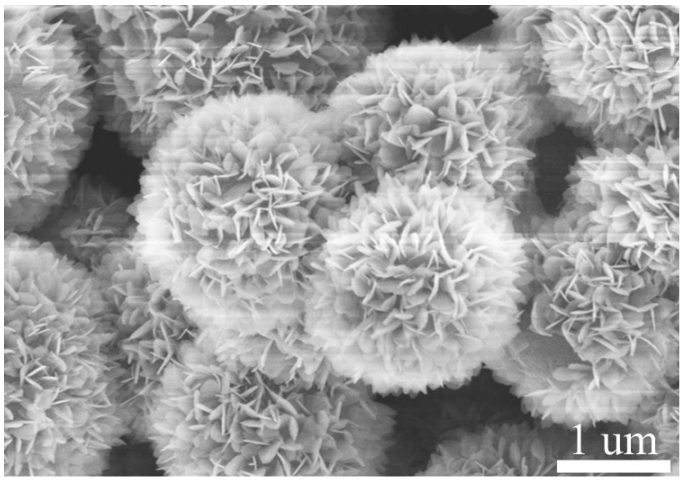

Figure S1. SEM image of product from solvothermal reaction.

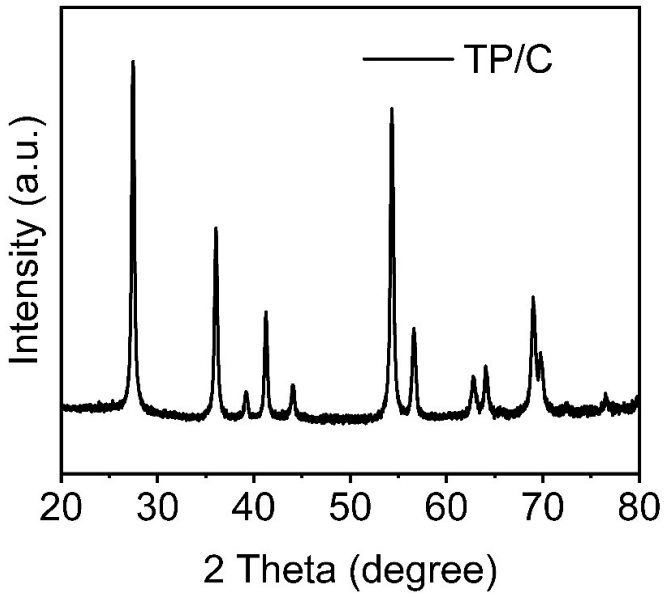

Figure S2. XRD pattern of TP/C.

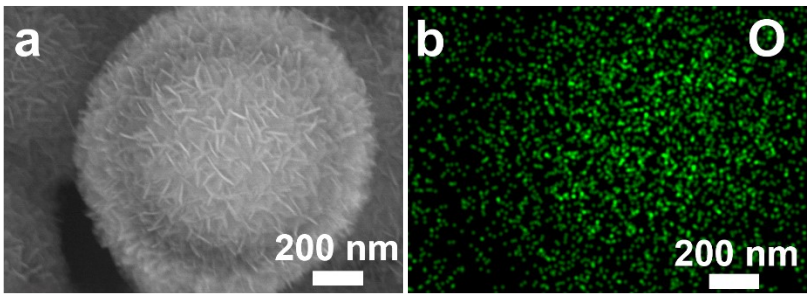

Figure S3. (a) SEM image and (b) corresponding elemental mapping of TNC/C-4.

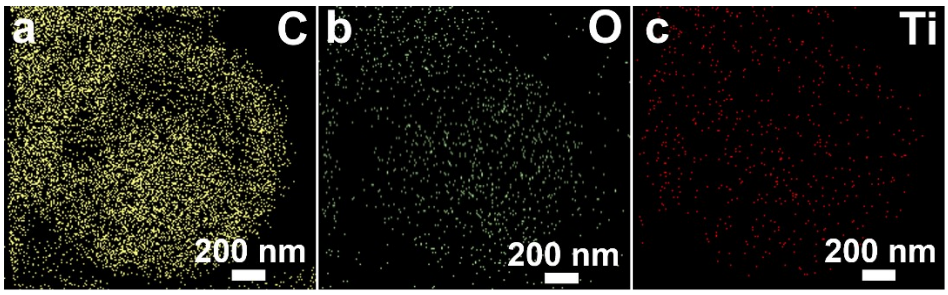

Figure S4. (a-c) The TEM-EDS elemental mapping images of TNC/C-4.

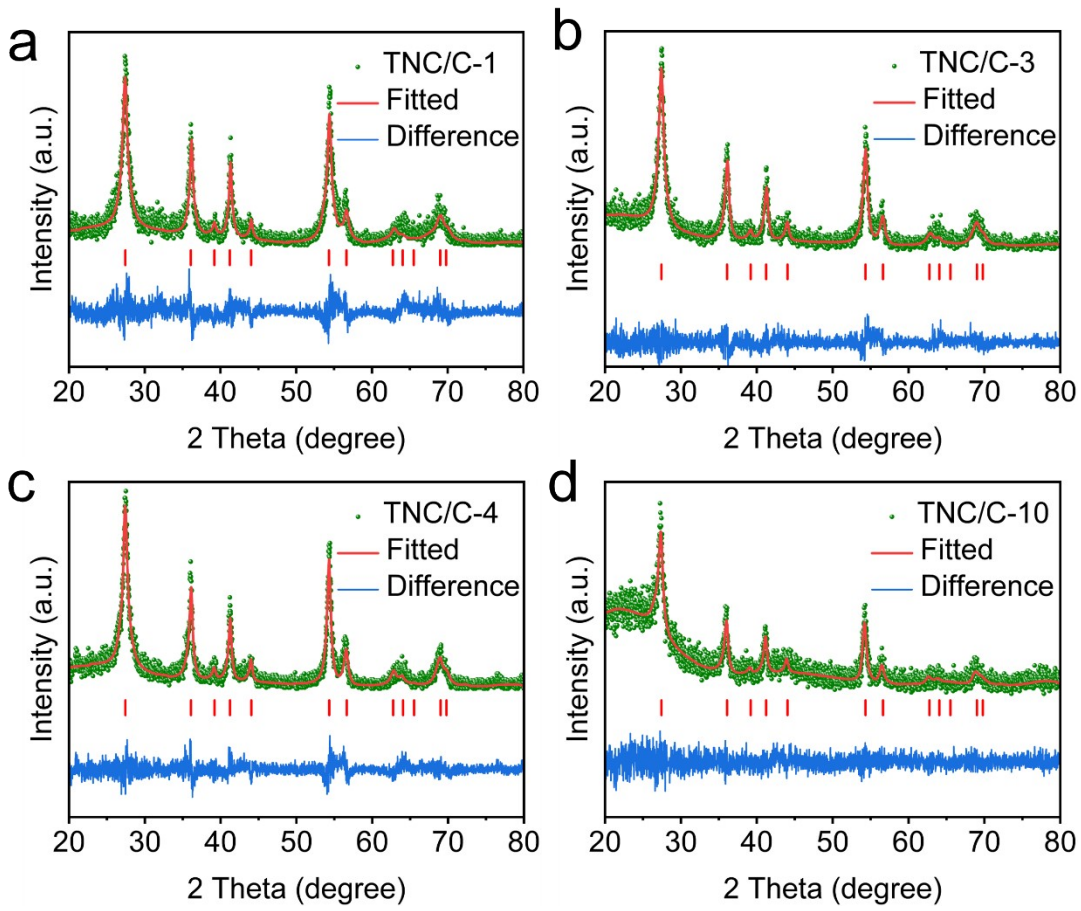

Figure S5. (a-d) Rietveld-refined XRD patterns of TNC/C-*X*.

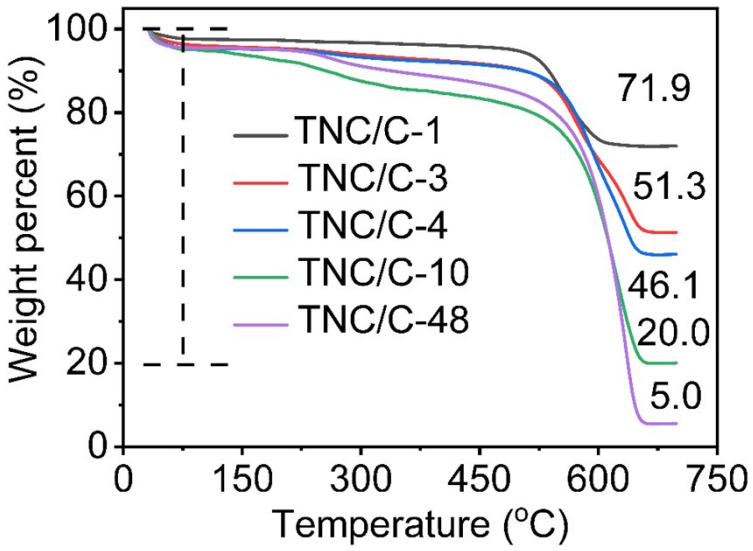

Figure S6. TGA curves of TNC/C-*X*.

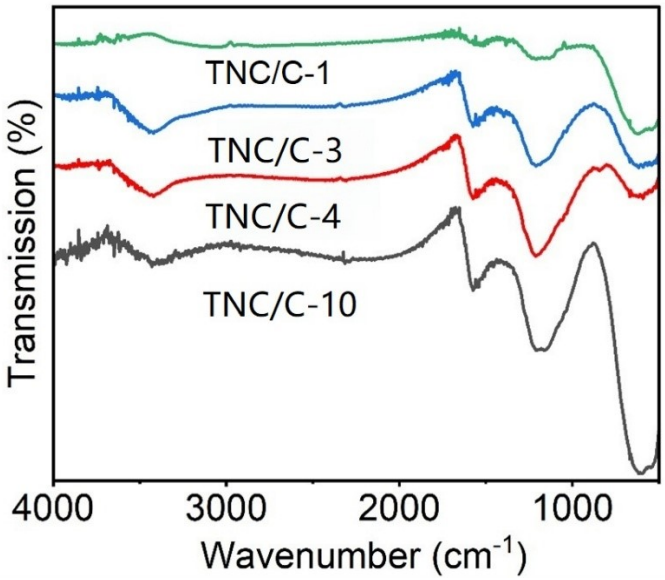

Figure S7. FT-IR spectra of TNC/C-*X*.

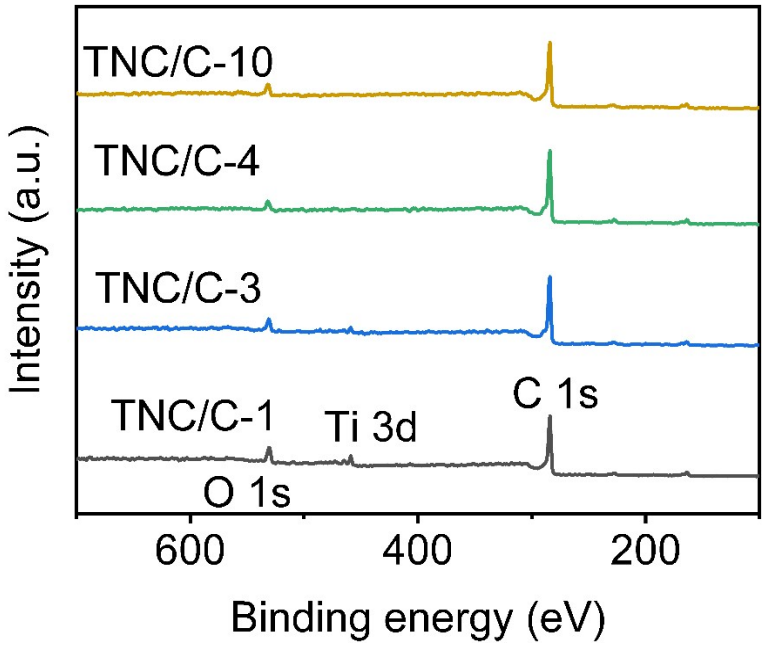

Figure S8. XPS survey spectra of TNC/C-*X*.

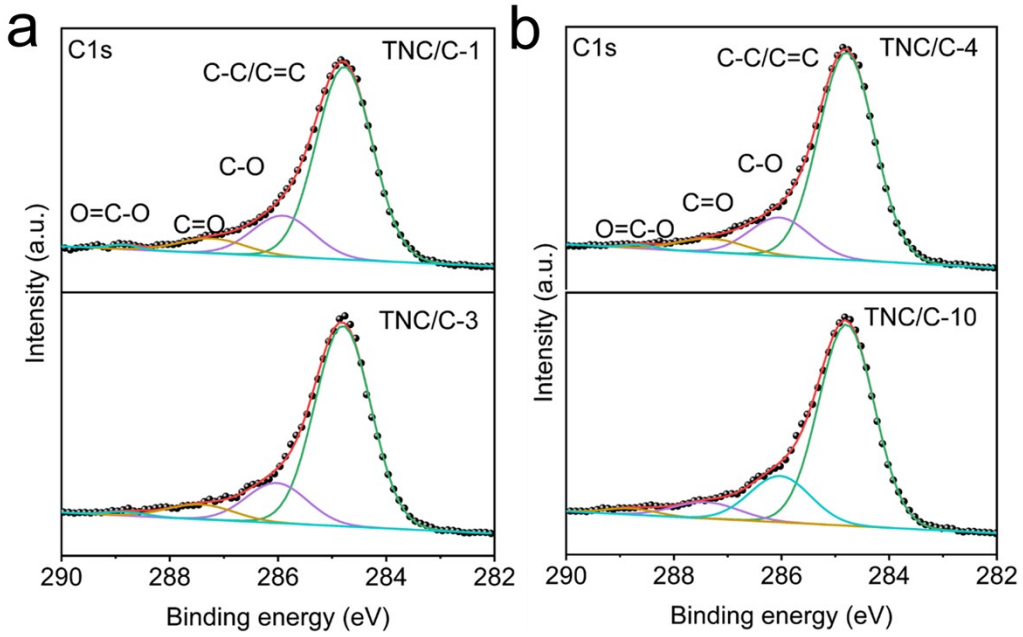

Figure S9. High-resolution C 1s XPS spectra of (a) TNC/C-1 and TNC/C-3, (b) TNC/C-4 and TNC/C-10.

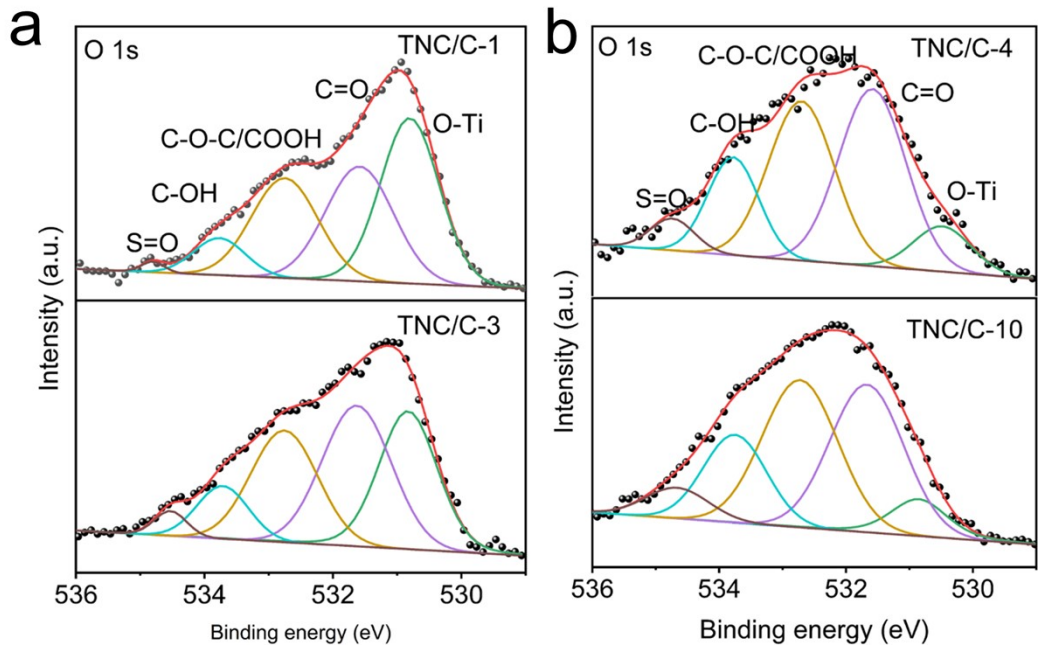

Figure S10. High-resolution O 1s XPS spectra of (a) TNC/C-1 and TNC/C-3, (b) TNC/C-4 and TNC/C-10.

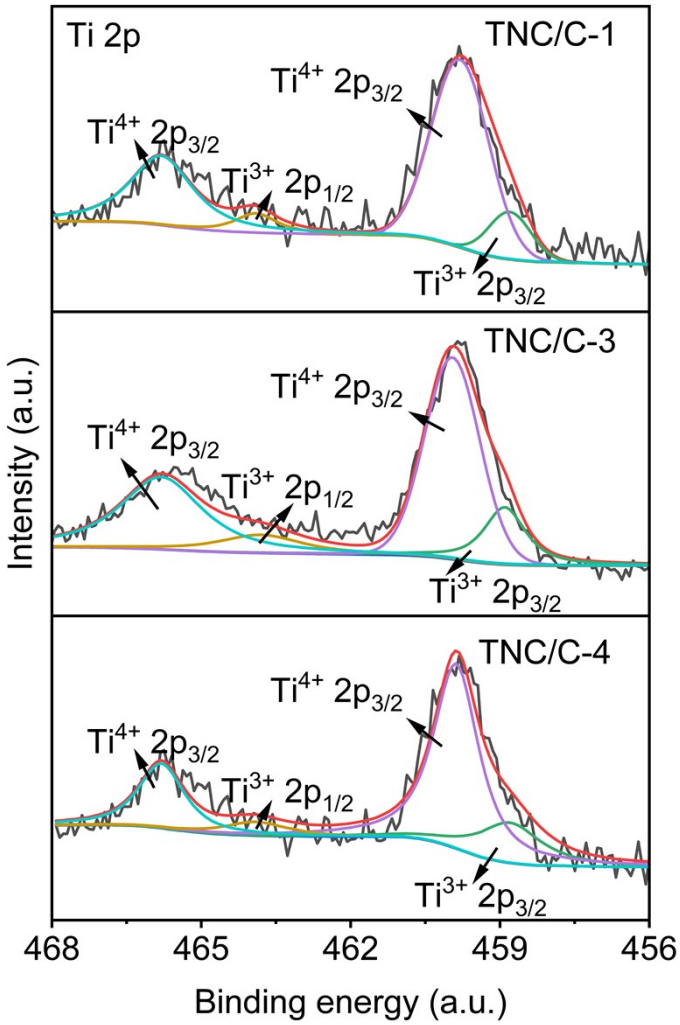

Figure S11. High-resolution Ti 2p XPS spectra of TNC/C-*X*.

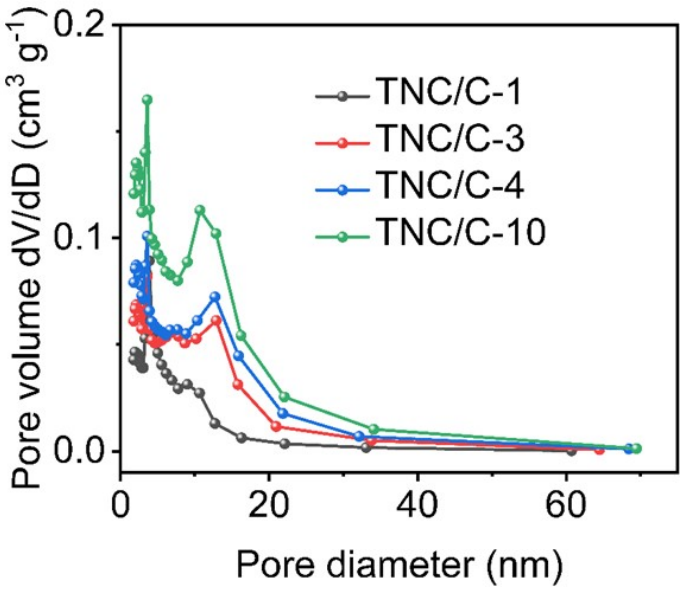

Figure S12. Pore size distribution curves of TNC/C-*X*.

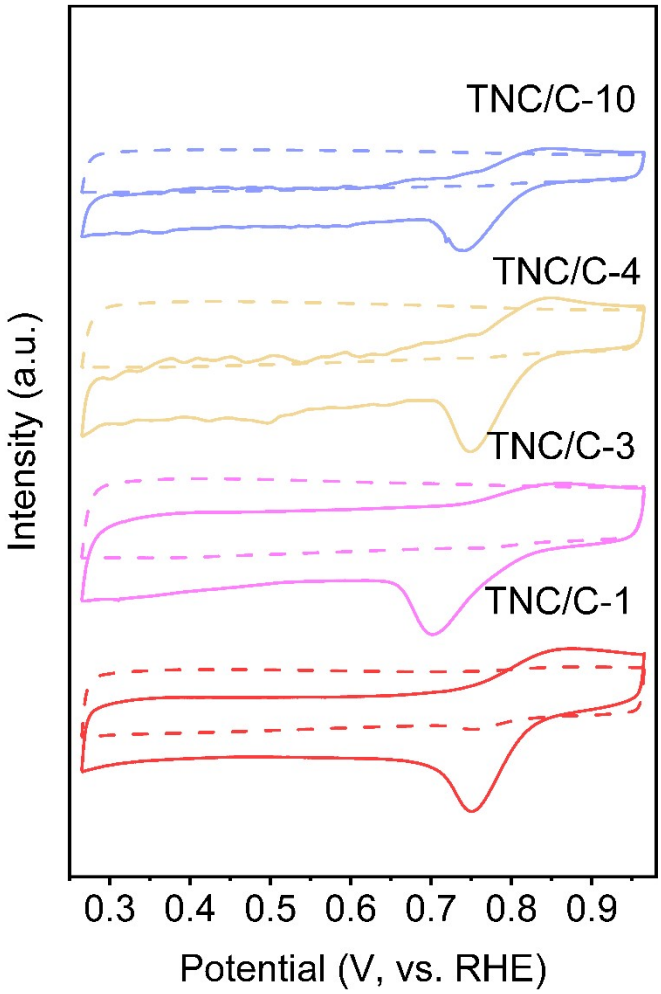

Figure S13. CV curves of TNC/C-1, TNC/C-3, TNC/C-4, and TNC/C-10 recorded in N_2-saturated (dashed lines) and O_2-saturated (solid lines) 0.1 M KOH at a scan rate of 50 mV s^{-1}.

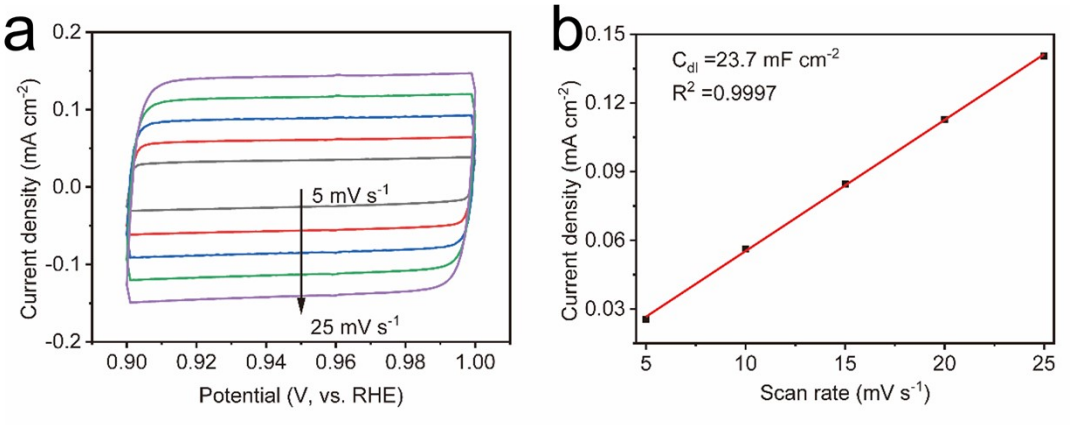

Figure S14. (a) CV curves of TNC/C-4 recorded in O_2-saturated 0.1 M KOH electrolyte at different scan rates. (b) Linear relationship between current density and scan rate used to determine the double-layer capacitance (C_{dl}).

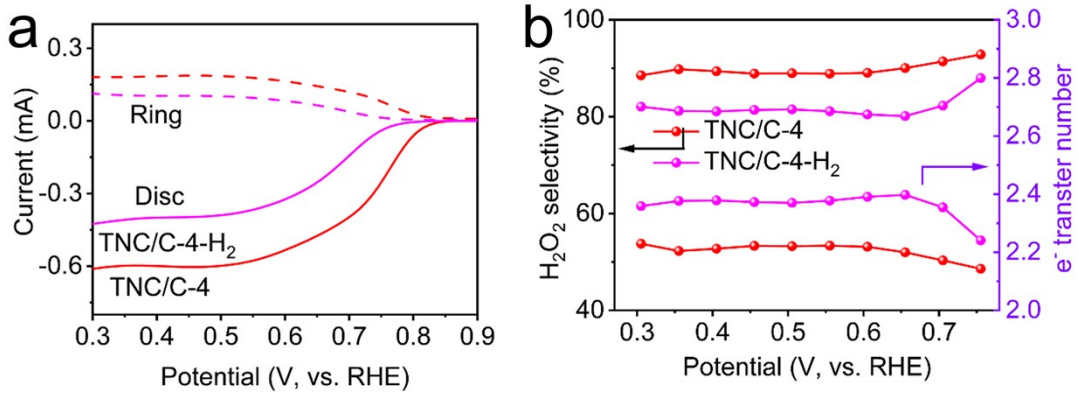

Figure S15. (a) RRDE polarization curves recorded at 1600 rpm in O_2-saturated 0.1 M KOH. (b) Corresponding H_2O_2 selectivity and electron-transfer number.

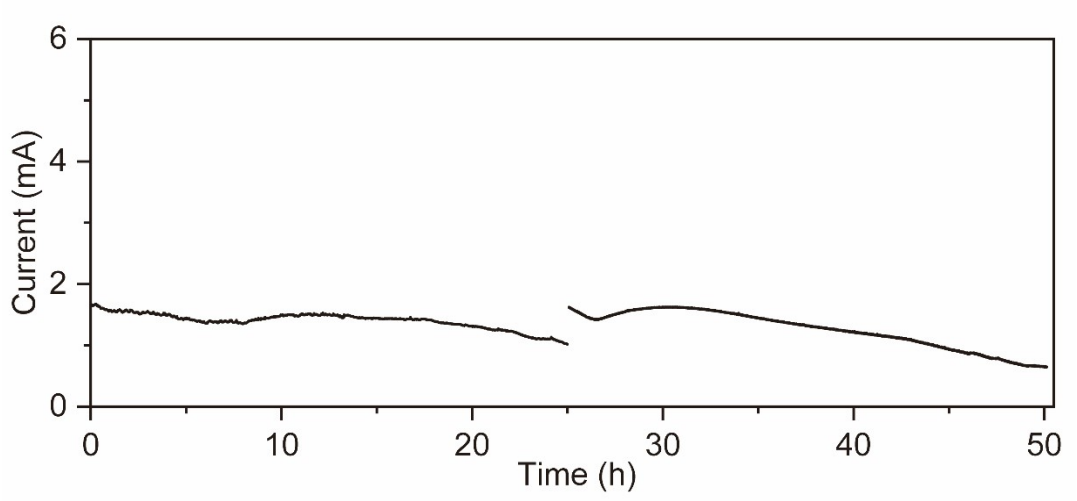

Figure S16. Chronoamperometry curve of TNC/C-4 recorded at 0.6 V in the flow cell.

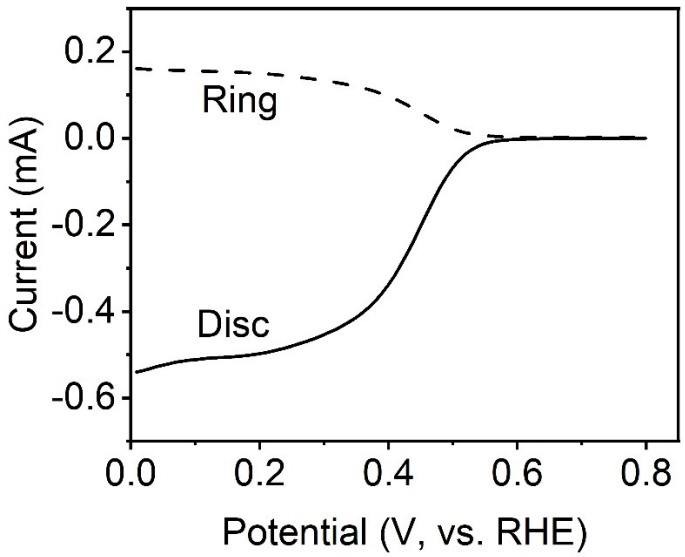

Figure S17. RRDE polarization curves of TNC/C-4 recorded at 1600 rpm in O_2-saturated 0.1 M Na_2SO_4.

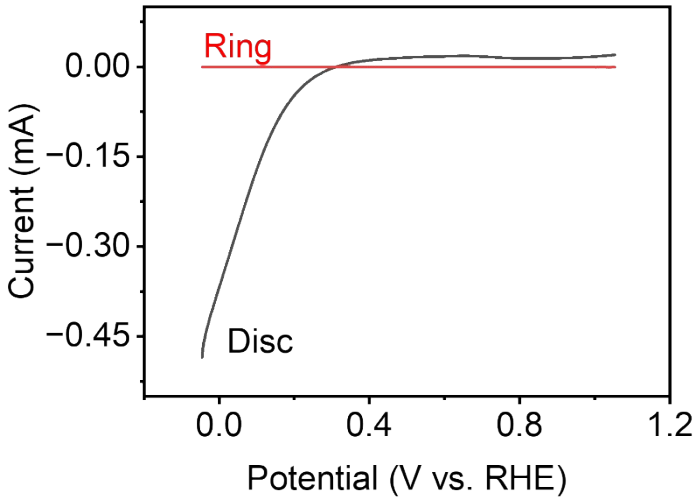

Figure S18. RRDE polarization curves recorded at 1600 rpm in O_2-saturated 0.1 M H_2SO_4.

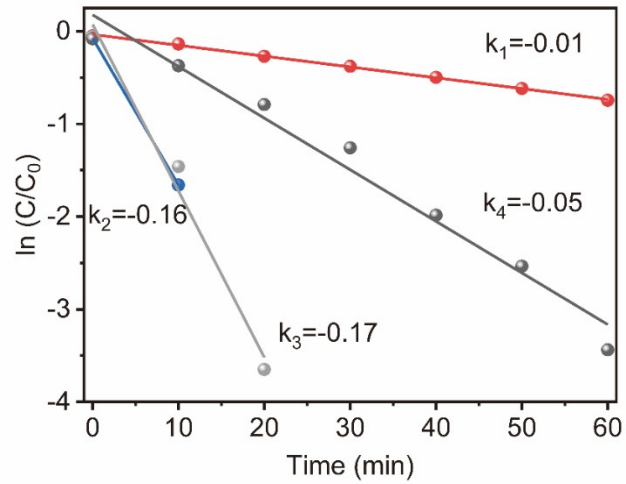

Figure S19. Comparison of apparent rate constants (k) for phenol degradation over TNC/C-4 under different conditions: 20 ppm without Fe^{2+} (k_1), 20 ppm electro-Fenton (k_2), 50 ppm electro-Fenton (k_3), and 200 ppm electro-Fenton (k_4).

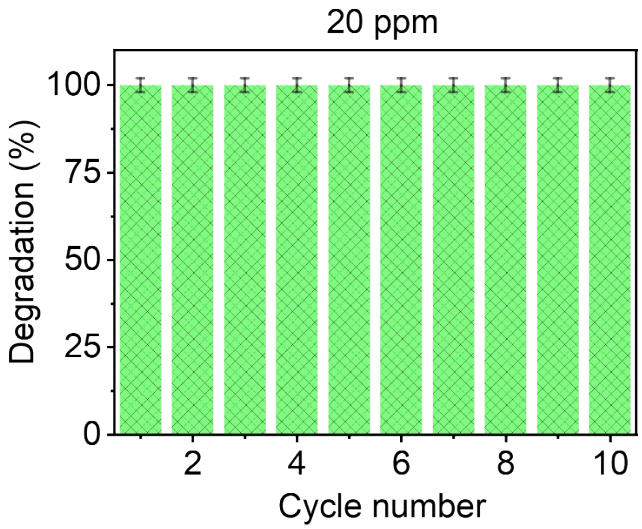

Figure S20. Cycling performance of TNC/C-4 for electro-Fenton degradation of 20 ppm phenol.

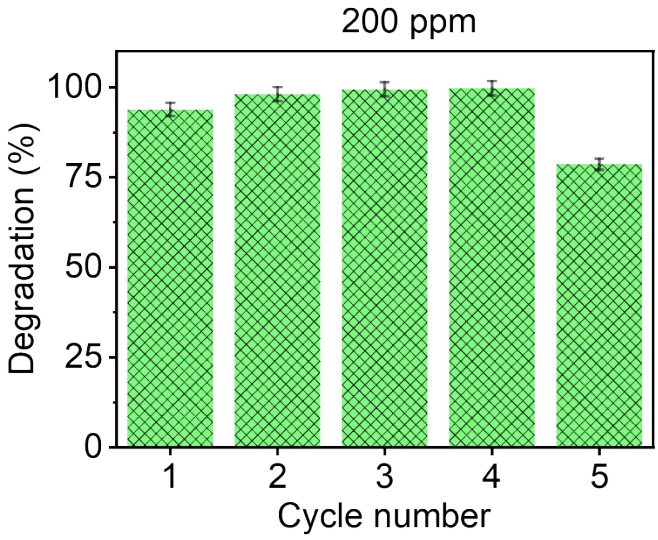

Figure S21. Cycling performance of TNC/C-4 for electro-Fenton degradation of 200 ppm phenol.

Table S1. Lattice constants of TNC/C-X obtained from Rietveld refinement.

Sample	Lattice parameter
TNC/C-1	a=b=4.5925 Å, c=2.9488 Å
TNC/C-3	a=b=4.5929 Å, c=2.9510 Å
TNC/C-4	a=b=4.5968 Å, c=2.9529 Å
TNC/C-10	a=b=4.6040 Å, c=2.9622 Å

Table S2. Specific surface area, pore volume, and pore size parameters of TNC/C-X.

Sample	Surface Area ($m^2\ g^{-1}$)	Pore Volume ($cm^3\ g^{-1}$)	Pore Size (nm)
TNC/C-1	434	0.76	7.0
TNC/C-3	669	1.51	9.0
TNC/C-4	794	1.94	9.5
TNC/C-10	1017	2.32	9.6

Table S3. Comparison of H_2O_2 production performance in this work and recent reports.

Electrocatalyst	Electrolyte	Selectivity (%)	Ref.
TNC/C-4	0.1 M KOH	92 (0.7 V)	Our works
S-mC	0.1 M KOH	90 (0.7 V)	1
P-NMG	0.1 M KOH	90 (0.7 V)	2
B-C	0.1 M KOH	95 (0.6 V)	3
G-MrBC	0.1 M KOH	95(0.6 V)	4
TiO_{2-x}/TiC	0.1 M KOH	90 (0.6 V)	5
NiO_x	0.1 M KOH	91 (0.6 V)	6
Au/TiO_2	0.1 M KOH	90 (0.5 V)	7

Table S4. ECSA of TNC/C-X estimated from C_{dl} (mF cm^{-2}).

Sample	TNC/C-1	TNC/C-3	TNC/C-4	TNC/C-10
ECSA	9.7	22.3	23.7	16.4

Table S5. Comparison of phenol degradation performance in electro-Fenton systems reported in previous studies.[8-14]

Electrocatalyst	Phenol	Removal efficiency	Ref.
TNC/C-4	200 ppm 0.1M Na_2SO_4	1 h 96.8%	Our works
OCNT	20 ppm 1M Na_2SO_4	1 h 99.9 %	8
FeN_2O_2-HPC	20 ppm pH=6.5	0.5 h 99.9 %	9
GCN	10 ppm pH=7	3 h 99.9 %	10
AC	50 ppm pH=3	2 h 100 %	11
PC-CNT	10 ppm pH=7	0.5 h 83.5 %	12
TiO_2-Fe^{3+}	200 ppm pH=7	1 h 82.48 %	13
N-EEGr-GFvv	50 ppm pH=3	0.8 h 91.1 %	14

References

1. J. Du, Y. Liu, M. Sun, J. Guan, A. Chen, B. Han, Angew. Chem. Int. Ed. 2025, 64, e202503385.
2. L. Han, Y. Wu, K. Fang, S. Sweeney, U. Roesner, M, Parrish, K, Patel, T, Walter, J, Piermattei, A, Trimboli, J, Lefler, C. Timmers, X. Yu, V. Jin, M. Zimmermann, A. Mathison, R. Urrutia, M. Ostrowski, G. Leone, Nat. Commun. 2023, 14, 4430.
3. Y. Wu, Y. Zhao, Q. Yuan, H. Sun, A. Wang, K. Sun, G. Waterhouse, Z. Wang, J. Wu, J. Jiang, M. Fan, Nat.Commun. 2024, 15,10843.
4. W. Cui, Z. Zhen, Y. Sun, X. Liu, J. Chen, S. Liu, H. Ren, Y. Lin, M. Wu, Z. Li Angew. Chem. Int. Ed. 2025, 64, e202423056.
5. Z. Xu, J. Liang, Y. Wang, K, Dong, X. Shi, Q. Liu, Y. Luo, T. Li, Y. Jia, A. Asiri, Z. Feng, Y. Wang, D. Ma, X. Sun, ACS Appl. Mater. Interfaces, 2021, 13, 33182.
6. Z. Wu, T. Wang, J. Zou, Y. Li, C. Zhang, ACS Catal. 2022, 12, 5911.
7. Y. He, Y. Wei, Z. Wang, T. Xia, F. Rao, Z. Song, R. Yu. Adv. Funct. Mater. 2024, 34, 2314654.
8. G. Zhu, X. Fan, Y. Yu, Y. Liu, X. Quan, Environ. Sci. Technol. 2024, 58, 19545.
9. Y. Lu, X. Qin, K. Wang, S. Chen, X. Quan, Sep. Purif. Technol. 2023, 320, 124196.
10. Y. Peng, Z. Bian, F. Wang, S. Li, S. Xu, H. Wang, J. Hazard. Mater. 2024, 462,

132797.

11. Y. Yang, S. Qiao, J. Zhou, X. Quan, Appl. Catal. B-Environ. 2019, 255, 117772.
12. O. Garcia-Rodriguez, A. Villot, H. Olvera-Vargas, C. Gerente, Y. Andres, O. Lefebvre, Carbon, 2020, 163, 265.
13. M. Haider, W. Jiang, J. Ha, H. Sharif, Y. Ding, H. Cheng, A. Wang, Appl. Catal. B-Environ. 2019, 256, 117774.
14. P. Cao, X. Quan, K. Zhao, S. Chen, H. Yu, J. Niu, J. Hazard. Mater. 2020, 382, 121102.